Normal modes and the Duschinsky mixing of the ground- and excited-state vibrations of the green fluorescent protein chromophore

ARTICLE *in* CHEMICAL PHYSICS LETTERS · NOVEMBER 2013

Impact Factor: 1.9 · DOI: 10.1016/j.cplett.2013.09.040

1 AUTHOR:

Ramachandran Gnanasekaran
Academy of Sciences of the Czech Republic
3 PUBLICATIONS **7** CITATIONS

Chemical Physics Letters 587 (2013) 61–67

Contents lists available at ScienceDirect

Chemical Physics Letters

journal homepage: www.elsevier.com/locate/cplett

Normal modes and the Duschinsky mixing of the ground- and excited-state vibrations of the green fluorescent protein chromophore

Ramachandran Gnanasekaran

Institute of Organic Chemistry and Biochemistry, Academy of Sciences of the Czech Republic, 16610 Prague, Czech Republic

ARTICLE INFO

Article history:
Received 18 July 2013
In final form 8 September 2013
Available online 23 September 2013

ABSTRACT

Ground- and excited-state vibrational frequencies were calculated for the chromophore of the green fluorescent protein (GFP) using the complete active space self-consistent field (CASSCF) method and detailed normal-mode analyses were carried out for ground and excited states. The mixing of the vibrational modes between the different states was studied by applying the Duschinsky effect by the expressing excited-state normal modes in terms of the ground-state normal modes. It was found that the low-frequency vibrational modes in the vertical excited state play a significant role in structural adjustment.

1. Introduction

The GFP serves as an important model system for photobiochemical-reaction investigations [1–4]. The wild-type GFP chromophore (*p*-hydroxybenzlidene imidazolinone) sheltered inside the beta barrel is formed by the internal cyclisation in the backbone of the Ser-Tyr-Gly sequence [5,6]. Following the excitation with light of wavelength 397 nm, the excited neutral chromophore converts to the unrelaxed anionic form by transferring the phenolic proton to the interacting residue Glu via a water molecule on a picosecond time scale [7,8]. Fang et al [9] explored the details of the initial events leading to proton transfer through femtosecond simulated Raman spectroscopy. In their letter, they showed the significance of the phenoxy-ring motions of the chromophore after excitation and the wagging motions enable the molecule to achieve the correct orientation for the transfer of the phenolic proton.

Later, Donato et al. explored in their letter the process of proton transfer in the GFP at atomic resolution by combining time-resolved mid-infrared spectroscopy and visible pump–dump–probe spectroscopy [10]. They found two time scales for proton transfer in the GFP after the absorption of light. The first was a 3 ps partial protonation time scale, which shifted the equilibrium position of the protons in the H-bonded network. This was followed by a deprotonation step, occurring at a later 10 ps time scale. Along with Winkler et al. [11], Donato et al. [10] supported the view that the GFP proton transfer potential energy surface can be seen as an adiabatic surface where the proton transfer is associated with vibrational cooling and concomitant small structural changes in the proton positions on the proton wire.

Here we made an attempt to explore the vibrational modes involved in the relaxation between the excited states S1 and S2. In our previous study, we showed the dielectric response to the photo excitation of the GFP chromophore and the role of confined water molecules with respect to their contributions [12]. Motivated by our letter and other results [7–12], thoretically we proceeded further to investigate the vibrational modes of the chromophore between the ground (S0), vertical excited state(S1) and stable excited state (S2). Although many groups have investigated the vibrational spectra of the GFP chromophore [9,10,13–18], an assignment of the vibrational spectra to different normal modes is lacking. In this Letter, we report a detailed normal-mode analysis of the neutral GFP chromophore in its S0, S1 and S2 excited states and interpret the change of the distribution of normal modes between the states. The mode mixing known as the Duschinsky effect [19] between the states (a) S0/S1, (b) S0/S2 and (c) S1/S2 was calculated to understand the vibrational-mode redistributions. The Duschinsky effect is usually applied to evaluate the Franck Condon factors [20–24]; considering the importance of the system, we have applied the effect to see the mixing of the modes between different states.

2. Computational details

The initial structure of the GFP chromophore was taken from the crystallographic structure 1EMA of the protein. Using the GAUSSIAN03 suite program [25], the ground-state geometry was optimised at the CASSCF level applying the 4-31G basis set. The active spaces are comprised of eight π electrons and eight π and π* orbitals. The harmonic vibrational frequencies in the S0, S1 and S2 states were calculated by the CASSCF method using the same basis set. The UMAT program [26] was used to carry out the

E-mail address: gtrama@gmail.com

0009-2614/$ - see front matter © 2013 Elsevier B.V. All rights reserved.
http://dx.doi.org/10.1016/j.cplett.2013.09.040

normal-mode analysis. The potential energy distributions (PEDs) of the normal modes were obtained from the force constants in Cartesian coordinates. Within the harmonic limit, the Duschinsky relation is given as

$$J = (L')^{-1}L,$$

where L is the eigen-vector matrix expressed in terms of suitably chosen (non-redundant) internal coordinates. The normal modes Q (S0 modes) and Q' (S1 modes) are related by the transformation $Q' = JQ$.

3. Results and discussion

The theoretically predicted geometrical parameters of the optimised ground (S0) and excited states (S2) are presented in Table 1. The table shows the bond distance and angles where a significant change occurs. Minor or no changes in the displacement are not listed. The elongation of the bond and the deviation of the angle depend on the change in the dipole moments of the system, which has been computationally found to be 0.34 Debye is comparable to the experimental value of 2.5 D [9]. This small discrepancy with the experimental value must have been caused by smaller basis set and active space considered. It should also be noted that a direct comparison of the free chromophore with its analogue embedded inside the protein may not be exact as the protein matrix influences the excitation process. As mentioned by Fang et al. [9], the chromophore modifies its conformation in the local environment mediated by the external proton–relay wire; the chemical bonds periodically vary their strengths and polarisability in response to the dynamical structural changes controlling the electron distribution over the two rings. However, our interest lies in understanding the vibrational mode mixing in a more qualitative way, if not quantitative.

In Tables 2–4, we report the details of the normal modes for the S0, S1 and S2 states. All the normal-mode analyses were carried out in the C1 point group symmetry, and there exist 60 numbers of vibrational frequencies. The calculated frequencies along with the potential-energy distribution (PED) are listed; the number in parentheses refers to the contribution of each mode on the total frequency. Any mode which contributes less than 10% is not listed in the table. In the PEDs, 'Ph' indicates the phenol-group moiety, 'imid' indicates the imidazolinone-group moiety, and 'exo' indicates the bridging (linking) atoms between the phenol and imidazolinone groups. As arises from the Table 2, most of the calculated frequencies correspond well with the experimental ones [13,15]. Deviations from experimental values are most probably caused by a combination of different factors, including the size the of active space used in the CASSCF calculation, the size of the basis set, the neglect of anharmonicity, the nature of the experimental conditions etc. The scale factors between the values 0.95 and 0.99 [27,28] are usually to correct the calculated frequencies to match the experiment values. It should be noted here that Andruniow [16] used the scale factor of 0.9 to report the calculated frequencies for the GFP chromophore.

Table 1
Geometrical parameters of the ground- and excited-state geometries.

Parameters	Ground state	Excited state
Bond distance		
C_1–C_2	1.406	1.439
C_2–C_3	1.396	1.497
C_3–C_4	1.389	1.417
C_4–C_5	1.372	1.342
C_6–C_1	1.382	1.368
C_3–H_{18}	1.068	1.065
C_5–O_{16}	1.372	1.369
C_2–C_7	1.462	1.381
C_7–C_8	1.342	1.436
C_8–N_9	1.427	1.337
N_9–C_{10}	1.290	1.395
C_{10}–N_{11}	1.400	1.387
N_{11}–C_{12}	1.374	1.371
C_{10}–H_{14}	1.064	1.059
Bond angle		
$\angle C_1$–C_2–C_3	118.0	116.3
$\angle C_6$–C_5–O_{16}	116.6	113.6
$\angle C_2$–C_7–H_{17}	115.5	117.8
$\angle C_7$–C_8–C_{12}	123.9	121.7
$\angle N_{11}$–C_{10}–N_9	112.9	108.8
$\angle N_{11}$–C_{10}–H_{14}	121.8	125.7
$\angle N_9$–C_8–C_{12}	107.8	109.7

The tables show that the region of 3000 cm^{-1} and above contains a contribution from well-known modes, mainly due to the stretching modes belonging to the OH, NH and CH modes. The region in between 1800 and 1200 cm^{-1} arises mainly from the contribution of the CO, CC, CN stretching, and COH, NCH, CCC, CCH, CNC bending modes. These modes mix/couple with others for a given particular frequency. This region is considered to be important (marker bands) because of the experimental (IR and Raman) evidence of numerous mode transitions [13,14]. Schellenberg et al. [14] mentioned about the dominance of the CN (imid) and CC (exo) stretching mode in the region 1565 cm^{-1} region. They assigned the modes depending on the intensities along with ab initio calculations. As we can see from the tables, the percentage of each mode is below 50% and the modes are mixed. Therefore, it is very difficult to select a mode for a particular frequency. Other modes like C=O and CC stretching [13] are quite noticeable within the range of marker bands. In the S0 state, the CC stretching mode occurs at a higher frequency region (~1750 cm^{-1}) than the C=O stretching mode when compared to the S1 and S2 states. In the excited-states, the C=O stretching mode occurs at ~1900 cm^{-1} and CC occurs at below that range. The region between 1600 and 1500 cm^{-1} was considered as a dominant band due to the CN and CC stretching mode in the reported resonance Raman spectra [14], mostly we found bending modes of CCH, CNH and NCH with little (10–20%) contribution from CC and CN stretching modes in Figure 1. However, they are dominant in the lower frequency range below 1500 cm^{-1}. The C–O (Ph) stretching modes occur around ~1350 cm^{-1}. In the region below 1200 cm^{-1}, we can see more out-of-plane bending and torsional modes apart from some contribution from the modes.

In order to understand the correlation of the normal modes between the S0, S1 and S2 states, the Duschinsky mixing was proposed. Figure 2 depicts the expansion of the S1-state normal modes (Q'') on the basis of the S0-state normal modes (Q). The X and Y axes are the numbers of the normal modes in the S1 and S0 states, respectively. A comparison of modes is provided in the PED of Tables 2 and 3 makes our understanding better. When the modes do not mix between the states (S0/S1/S2), the enhancement of Fanck Condon factor is visible in the figures (check the color code) as the same modes overlap. For example, the first eight frequencies come mainly from the OH, NH and CH modes, and are reflected in the color change. Mode mixing involves many nonlinearities; for example, CC stretching mode mixes more (~50%) with the CC torsion mode in the vertical excitation. Interestingly, we can notice many similarities in the Duschinsky mixing from the figures and Supplementary details. As mentioned by [14], the OH stretching mode does not mix or couple with any other modes, so that it is free to detach in the excited state. Similarly, Figure 3 depicts the expansion of the S2 normal modes (Q') on the basis of the S0-state normal modes (Q). Figure 4 shows the expansion of the S2 normal modes (Q') on the basis of S1 normal modes (Q''). The corresponding data of these Figures 2–4 were

Table 2
Ground state (S0) vibrational frequencies and PED of GFP chromophore.

No	Expt frequencies	Calculated	PED
A			
1	–	3521.1	*νOH*(*Ph*) (99)
2	–	3470.8	*νNH*(*imid*) (92)
3	–	3293.8	*νCH*(*Ph*) (95)
4	–	3280.9	*νCH*(*Ph*) (84), *νCH*(*Ph*) (14)
5	–	3257.0	*νCH*(*Ph*) (93)
6	–	3253.0	*νCH*(*Ph*) (75), *νCH*(*Ph*) (14)
7	–	3250.2	*νCH*(*imid*) (99)
8	–	3241.3	*νCH*(*exo*) (90)
9	–	1756.6	*νCC*(*exo*) (34), *δCCH*(*exo*) (18)
10	–	1747.9	*νCC*(*Ph*) (30), *νCC*(*Ph*) (16), *δCCH*(*Ph*) (12)
11	–	1733.5	*νCC*(*Ph*) (15), *δCCH*(*Ph*) (15), *νCC*(*exo*) (10)
12	1697.0(R)	1708.6	*νC═O*(*imid*) (44), *δCNH*(*imid*) (12), *νCC*(*imid*) (10)
13	1643.0(R)	1674.8	*δCOH*(*Ph*) (29), *δCCH*(*Ph*) (16), *δCCH*(*Ph*) (16)
14	1603.0(R)	1613.6	*δNCH*(*imid*) (29), *νCN*(*imid*) (28), *δCNH*(*imid*) (22)
15	1591.0(R)	1591.5	*δCCH*(*Ph*) (29), *δCOH*(*Ph*) (17), *νCC*(*Ph*) (11), *δCCH*(*Ph*) (10)
16	1561.0(R)	1538.4	*δCNH*(*imid*) (41), *δNCH*(*imid*) (17)
17	1514.0(IR)	1532.4	*δCCH*(*Ph*) (28), *δCCH*(*Ph*) (19), *δCCH*(*exo*) (11)
18	1449.0(R)	1480.0	*δCCC*(*exo*) (36), *δCCH*(*exo*) (29)
19	1430.0(IR)	1445.9	*δCCH*(*Ph*) (31), *δCOH*(*Ph*) (19)
20	1393.0(IR)	1390.2	*νCN*(*imid*) (52), *δNCH*(*imid*) (35)
21	1362.0(IR)	1347.7	*νC–O*(*Ph*) (25), *νCC*(*Ph*) (18), *νCC*(*Ph*) (16), *νCC*(*Ph*) (14)
22	1317.0(R)	1320.3	*δCCH*(*Ph*) (25), *νCC*(*exo*) (16), *δCCC*(*Ph*) (12)
23	1301.0(IR)	1311.0	*δCCH*(*Ph*) (21), *δCCC*(*Ph*) (15), *νCC*(*exo*) (13), *νCC*(*Ph*) (13)
24	1234.0(R)	1252.9	*νCC*(*imid*) (15), *δCNC*(*imid*) (15), *νNC*(*imid*) (14)
25	1230.0(IR)	1203.5	*νCC*(*Ph*) (11
26	1178.0(R)	1151.2	*γCH*(*Ph*) (36), *γCH*(*exo*) (23), *γCH*(*Ph*) (12)
27	1138.0(IR)	1130.1	*γCH*(*exo*) (47), *τCC*(*exo*) (12)
28	–	1125.8	*νCN*(*imid*) (37), *νNH*(*imid*) (11)
29	1109.0(IR)	1115.8	*δCCC*(*Ph*) (31), *νCC*(*Ph*) (20), *νCC*(*Ph*) (18), *νCC*(*Ph*) (11)
30	–	1092.4	*γCH*(*Ph*) (32), *γCH*(*Ph*) (30), *τCC*(*Ph*) (12), *τCC*(*Ph*) (11)
31	–	1089.4	*νCC*(*Ph*) (21), *νCC*(*Ph*) (19), *νCC*(*Ph*) (15)
32	1039.0(R)	1057.0	*δNCC*(*imid*) (22), *νCN*(*imid*) (16), *νNC*(*imid*) (16), *νCN*(*imid*) (10)
33	1010.0(IR)	1008.2	*γCH*(*Ph*) (52), *γCH*(*Ph*) (22)
34	–	975.5	*γCH* (47), *τNC*(*imid*) (28), *τCN*(*imid*) (14)
35	936.0(IR)	945.0	*νNH*(*imid*) (29), *γNH* (23)
36	900.0 (IR)	940.1	*γCH*(*Ph*) (33), *γCH*(*Ph*) (31)
37	851.0(IR)	887.0	*νNH*(*imid*) (24), *γNH* (20), *δCNC*(*imid*) (19)
38	840.0(IR)	851.3	*νCC*(*Ph*) (16), *νNH*(*imid*) (13), *δCCC*(*Ph*) (12), *γNH* (11)
39	823.0(IR)	833.7	*τCO*(*Ph*) (66)
40	–	820.8	*νCN*(*imid*) (22), *δCCC*(*exo*) (12)
41	–	817.4	*γCO*(*imid*) (39), *γCC*(*imid*) (25)
42	781.0(IR)	808.9	*νNH*(*imid*) (26), *γNH* (20)
43	754.0(IR)	803.4	*γCC*(*Ph*) (19), *τCC*(*Ph*) (19), *τCO*(*Ph*) (14), *νNH*(*imid*) (11), *γCO*(*Ph*) (11)
44	711.0(IR)	715.2	*δCCC*(*Ph*) (41), *δCCN*(*imid*) (13)
45	654.0(IR)	699.6	*δCCC*(*Ph*) (18), *γCO*(*imid*) (17), *τCC*(*exo*) (11)
46	636.0(IR)	683.7	*γCO*(*imid*) (16), *δCCN*(*imid*) (14), *νNH*(*imid*) (11), *τNC*(*imid*) (11)
47	608.0(IR)	621.6	*δCCC*(*Ph*) (14), *νNH*(*imid*) (12), *δCCN*(*imid*) (12), *νNC*(*imid*) (11), *δCC═O*(*imid*) (11)
48	575.0(IR)	611.1	*γCC*(*Ph*) (33), *γCO*(*Ph*) (24)
49	512.0(IR)	526.4	*δCC═O*(*imid*) (30), *δCCC*(*Ph*) (26)
50	–	496.5	*τCC*(*exo*) (29), *τNC*(*imid*) (15), *τCN*(*imid*) (13)
51	–	480.3	*τCC*(*Ph*) (37), *τCC*(*Ph*) (21)
52	–	470.8	*δCCO*(*Ph*) (63), *δCCC*(*Ph*) (12)
53	–	387.3	*γCC*(*imid*) (21), *τNC*(*imid*) (17), *γCO*(*imid*) (16), *γCC*(*Ph*) (16), *τCC*(*Ph*) (14)
54	–	300.8	*δCCC*(*Ph*) (44), *δNCC*(*imid*) (14), *δCCC*(*exo*) (10)
55	–	283.1	*τCN*(*imid*) (36), *τNC*(*imid*) (26), *γNH* (12)
56	–	245.1	*δNCC*(*imid*) (38), *νCC*(*exo*) (12), *νCC*(*imid*) (10)
57	–	229.3	*τCC*(*exo*) (25), *τCC*(*Ph*) (15), *γCC*(*imid*) (12)
58	–	160.4	*δCCC*(*Ph*) (26), *δCCC*(*exo*) (26), *δNCC*(*imid*) (17)
59	–	130.7	*τCC*(*exo*) (35), *τCC*(*exo*) (15)
60	–	108.5	*τCC*(*exo*) (45), *τCC*(*Ph*) (21)

The number in parentheses refers to the precent contribution each mode has on the frequency.
Only modes contributing more than 10% are listed.
The experimental values were taken from the Refs. [13,15].
R – Raman; IR – Infrared.

tabulated in the Supplementary Material Tables SP (1–3). These are more important for our discussion on vibrational relaxation between the excited states. The calculated energy difference between the S1 and S2 states is 5590.1 cm^{-1} within this difference, it is interesting to see the redistribution of modes. From Tables 3 and 4, we can note that the difference in the vibrational energy levels between the S1 and S2 states is within 50 cm^{-1} the two imaginary frequencies are exceptions. Therefore, the mode mixing or redistribution occurs within this capacity of energy. Figures 2–4 show that in the higher frequency range of 4050–3000 cm^{-1}, the normal modes like OH and C–H stretching are more localised, and the actual mode mixing starts from Q''_{10} indicating that the

Table 3
Vertical excited-state (s1) vibrational *frequencies* and PED of GFP chromophore.

No	Frequencies	PED
1	4024.1	*νOH*(*Ph*) (100)
2	3924.3	*νNH*(*imid*) (99)
3	3457.2	*νCH*(*imid*) (99)
4	3418.8	*νCH*(*Ph*) (97)
5	3399.3	*νCH*(*Ph*) (96)
6	3357.5	*νCH*(*Ph*) (93)
7	3346.0	*νCH*(*Ph*) (97)
8	3324.7	*νCH*(*exo*) (96)
9	1902.6	*νC*=*O*(*imid*) (66)
10	1842.6	*νCC*(*exo*) (57)
11	1786.5	*νCC*(*Ph*) (23), *νCC*(*Ph*) (20), *δCCH*(*Ph*) (12)
12	1699.5	*νCC*(*Ph*) (27), *νCC*(*Ph*) (23)
13	1666.0	*νCC*(*Ph*) (27), *δCCH*(*Ph*) (24), *νCN*(*imid*) (11)
14	1641.8	*νCN*(*imid*) (36), *δNCH*(*imid*) (20)
15	1560.2	*δCCH*(*Ph*) (26), *δCCH*(*Ph*) (19)
16	1552.8	*δCCH*(*Ph*) (58), *νCC*(*Ph*) (13)
17	1532.3	*δCNH*(*imid*) (60), *νCN*(*imid*) (18)
18	1512.8	*δCCH*(*exo*) (26), *δCCC*(*exo*) (10)
19	1451.8	*δNCH*(*imid*) (15), *δCCH*(*exo*) (14), *δCCC*(*exo*) (13), *δCCH*(*Ph*) (12), *δCCH*(*Ph*) (10)
20	1421.9	*δNCH*(*imid*) (33), *νCN*(*imid*) (26), *νNC*(*imid*) (11)
21	1375.7	*νC*−*O*(*Ph*) (39), *δCCC*(*Ph*) (18)
22	1314.6	*δCCH*(*Ph*) (32), *δCCH*(*Ph*) (24)
23	1267.1	*δCOH*(*Ph*) (57)
24	1239.0	*νNC*(*imid*) (36), *δCNC*(*imid*) (16), *δNCH*(*imid*) (14), *δCC*=*O*(*imid*) (12)
25	1202.6	*νCC*(*Ph*) (24), *δCCH*(*Ph*) (16), *δCOH*(*Ph*) (12)
26	1134.3	*νCN*(*imid*) (49), *δCNH*(*imid*) (14)
27	1123.7	*δCCC*(*Ph*) (43), *νCC*(*Ph*) (15), *νCN*(*imid*) (10)
28	1121.0	*γCH*(*Ph*) (49), *γCH*(*Ph*) (33)
29	1049.7	*δCNC*(*imid*) (41), *νCN*(*imid*) (21)
30	954.0	*γCH*(*Ph*) (32), *γCH*(*Ph*) (21), *γCH*(*Ph*) (18)
31	931.0	*γCH*(*Ph*) (26), *γCH*(*Ph*) (22), *γCH*(*Ph*) (14)
32	927.1	*νCC*(*exo*) (16), *νCC*(*Ph*) (13), *νCN*(*imid*) (13), *νNC*(*imid*) (10)
33	906.2	*νCC*(*imid*) (44), *νCN*(*imid*) (11), *νCN*(*imid*) (10)
34	891.3	*γCH*(*exo*) (43), *γCO*(*imid*) (19), *γCC*(*imid*) (12), *γCH*(*Ph*) (11)
35	885.3	*νCN*(*imid*) (23), *νC*−*O*(*Ph*) (15), *νCC*(*Ph*) (10)
36	852.6	*γCO*(*imid*) (43), *γCH*(*Ph*) (11)
37	847.7	*δCCC*(*Ph*) (16), *νCC*(*Ph*) (14), *νCN*(*imid*) (13)
38	820.9	*γCH*(*Ph*) (33), *γCH*(*Ph*) (26), *γCO*(*Ph*) (13)
39	760.1	*γCH* (74), *τCN*(*imid*) (11), *τNC*(*imid*) (11)
40	737.8	*δCCN*(*imid*) (49), *νC*=*O*(*imid*) (10)
41	703.9	*γCO*(*Ph*) (35), *γCC*(*Ph*) (25), *τCC*(*Ph*) (23)
42	702.1	*δCCC*(*Ph*) (74)
43	690.3	*γNH* (65), *τNC*(*imid*) (14), *γCC*(*imid*) (12)
44	650.2	*δCCC*(*Ph*) (25), *δCC*=*O*(*imid*) (19)
45	629.0	*τNC*(*imid*) (56), *τCN*(*imid*) (16), *γNH* (12)
46	553.2	*γCC*(*Ph*) (39), *γCO*(*Ph*) (33)
47	531.7	*δCC*=*O*(*imid*) (31), *δCCC*(*Ph*) (23), *νCC*(*exo*) (14)
48	446.7	*δCCO*(*Ph*) (64), *δCCC*(*Ph*) (13)
49	426.8	*τCO*(*Ph*) (93)
50	375.0	*τCC*(*Ph*) (33), *γCO*(*Ph*) (19), *γCH*(*Ph*) (16), *τCC*(*Ph*) (13)
51	348.6	*γCC*(*imid*) (40), *γCO*(*imid*) (25), *γNH* (13)
52	309.7	*δCCC*(*Ph*) (22), *νCC*(*exo*) (13), *δCCO*(*Ph*) (12), *νCC*(*exo*) (12)
53	275.9	*τCC*(*Ph*) (39), *γCH*(*Ph*) (21), *τCC*(*Ph*) (21)
54	221.1	*δNCC*(*imid*) (35), *δCC*=*O*(*imid*) (16), *νCC*(*exo*) (14), *δCCC*(*Ph*) (12)
55	198.0	*τCN*(*imid*) (36), *γCC*(*imid*) (33), *τNC*(*imid*) (13)
56	132.7	*τCC*(*Ph*) (45), *τCC*(*Ph*) (10)
57	90.3	*δCCC*(*Ph*) (16), *νCC*(*Ph*) (13), *δCCC*(*exo*) (12), *δNCC*(*imid*) (11)
58	13.0	*γCH*(*exo*) (56), *τCC*(*exo*) (16), *γCC*(*Ph*) (14)
59	−83.4	*τCN*(*imid*) (31), *γCO*(*Ph*) (12), *γCC*(*Ph*) (12), *τNC*(*imid*) (12)
60	−831.2	*νCC*(*Ph*) (20), *νCC*(*Ph*) (18), *νCC*(*exo*) (16), *νCC*(*Ph*) (12)

Table 4
Optimized excited-state (S2) vibrational frequencies, and PED of GFP chromophore.

No	Frequencies	PED
1	4013.1	*νOH*(*Ph*) (100)
2	3918.1	*νNH*(*imid*) (99)
3	3523.3	*νCH*(*imid*) (99)
4	3453.4	*νCH*(*Ph*) (99)
5	3403.5	*νCH*(*Ph*) (96)
6	3355.3	*νCH*(*exo*) (52), *νCH*(*Ph*) (46)
7	3349.2	*νCH*(*Ph*) (50), *νCH*(*exo*) (48)
8	3336.8	*νCH*(*Ph*) (99)
9	1916.7	*νC*=*O*(*imid*) (68)
10	1825.6	*νCC*(*exo*) (32), *νCC*(*exo*) (17)
11	1700.2	*νCC*(*Ph*) (38), *νCN*(*imid*) (11), *νCC*(*exo*) (10)
12	1667.0	*νCC*(*Ph*) (20), *δCCH*(*Ph*) (14), *νCC*(*Ph*) (12)
13	1610.7	*νCC*(*Ph*) (18), *δCCH*(*Ph*) (17), *δCCH*(*Ph*) (10)
14	1596.6	*δCCH*(*exo*) (30), *δCCC*(*exo*) (21), *νCN*(*imid*) (16), *δCCH*(*Ph*) (11)
15	1554.1	*δCNH*(*imid*) (65), *νCN*(*imid*) (11)
16	1520.9	*δCCH*(*Ph*) (30), *δCCH*(*Ph*) (23), *δCCH*(*Ph*) (13)
17	1506.4	*δNCH*(*imid*) (24), *δCCH*(*exo*) (11)
18	1467.2	*δCCH*(*Ph*) (44), *δNCH*(*imid*) (15)
19	1434.6	*νCC*(*exo*) (17), *δCCH*(*Ph*) (15), *δCCH*(*exo*) (13), *δNCH*(*imid*) (12)
20	1401.6	*νCC*(*imid*) (16), *νNC*(*imid*) (13), *νCC*(*Ph*) (13), *δCNC*(*imid*) (13)
21	1365.8	*δCCH*(*Ph*) (30), *νC*−*O*(*Ph*) (23), *δCOH*(*Ph*) (17)
22	1323.5	*δCNC*(*imid*) (14), *νNC*(*imid*) (12), *νCC*(*Ph*) (11)
23	1260.9	*δCOH*(*Ph*) (35), *δCCH*(*Ph*) (20), *νC*−*O*(*Ph*) (14)
24	1226.9	*νCC*(*Ph*) (21), *δCOH*(*Ph*) (17), *δCCH*(*Ph*) (14), *νCC*(*Ph*) (11)
25	1223.3	*νCN*(*imid*) (29), *νNC*(*imid*) (22), *νCC*(*exo*) (13)
26	1159.7	*δNCH*(*imid*) (21), *νCN*(*imid*) (20)
27	1104.0	*νCC*(*Ph*) (41)
28	1051.4	*δCCC*(*Ph*) (41), *νCC*(*Ph*) (22)
29	1020.1	*γCH*(*Ph*) (76)
30	997.1	*γCH*(*Ph*) (52), *γCH*(*Ph*) (20), *τCC*(*Ph*) (11)
31	966.5	*νCN*(*imid*) (28), *νCC*(*Ph*) (21), *δCCN*(*imid*) (15)
32	927.8	*γCH*(*exo*) (66)
33	907.0	*δCNC*(*imid*) (33), *νCN*(*imid*) (12)
34	873.5	*νCC*(*imid*) (28), *νCN*(*imid*) (20), *δCNC*(*imid*) (10)
35	851.4	*γCO*(*imid*) (59), *γNH* (16)
36	826.9	*νC* − *O*(*Ph*) (15), *νCC*(*Ph*) (13), *δCCC*(*Ph*) (12)
37	800.4	*γCH*(*Ph*) (58), *γCO*(*Ph*) (16), *γCH*(*Ph*) (16)
38	783.7	*νCC*(*Ph*) (29), *νCN*(*imid*) (19)*i δCCC*(*Ph*) (11)
39	746.5	*δCCN*(*imid*) (38)
40	709.0	*γNH* (64), *τNC*(*imid*) (19)
41	702.5	*γCC*(*Ph*) (29), *γCH*(*Ph*) (21), *γCO*(*Ph*) (19)
42	668.7	*δCCC*(*Ph*) (*51*), *νCC*(*Ph*) (12)
43	639.3	*γCH*(*Ph*) (46), *γCO*(*Ph*) (19), *τCC*(*Ph*) (16)
44	616.7	*δCC*=*O*(*imid*) (35)
45	549.9	*τNC*(*imid*) (29), *τCN*(*imid*) (25), *γCC*(*imid*) (20), *γCO*(*imid*) (14)
46	494.5	*γCC*(*Ph*) (34), *γCH*(*Ph*) (17), *γCO*(*Ph*) (15)
47	486.8	*δCCC*(*Ph*) (30), *δCC*=*O*(*imid*) (21)
48	435.8	*δCCO*(*Ph*) (51), *δCCC*(*Ph*) (16)
49	430.2	*τCO*(*Ph*) (20), *τCC*(*exo*) (12), *τCC*(*Ph*) (11), *γCO*(*Ph*) (11)
50	410.4	*τCO*(*Ph*) (79)
51	364.1	*τCC*(*Ph*) (26), *τCC*(*Ph*) (13), *γCC*(*imid*) (12), *γCH*(*Ph*) (12)
52	310.5	*τCC*(*Ph*) (39), *γCO*(*Ph*) (11)
53	296.0	*δCCC*(*Ph*) (29), *νCC*(*exo*) (13), *δCCO*(*Ph*) (11)
54	247.6	*τCN*(*imid*) (36), *τNC*(*imid*) (21)
55	217.0	*δNCC*(*imid*) (36), *δCCC*(*Ph*) (15), *δCC*=*O*(*imid*) (11)
56	128.2	*τCC*(*Ph*) (24), *τCC*(*Ph*) (21), *γCC*(*imid*) (11)
57	109.4	*δCCC*(*exo*) (35), *δNCC*(*imid*) (25), *δCCC*(*Ph*) (19)
58	75.9	*γCH* (45), *τCN*(*imid*) (28), *τNC*(*imid*) (24)
59	50.8	*γCH* (46), *τNC*(*imid*) (28), *τCN*(*imid*) (24)
60	30.7	*γCH* (46), *τNC*(*imid*) (27), *τCN*(*imid*) (24)

redistribution of modes occurs in the lower frequency region. In the low-frequency region, along with stretching modes, in-plane, out-of-plane and torsion modes gain more importance in energy distributions. It is a consequence of the collective redistribution of the energies (coherent nature) belonging to these modes and responsible for the shift of the equilibrium positions as well as for the detachment of the phenolic proton. This information on the energy relaxation between the modes is provided in Figure 4 and the Supplementary Table SP 3.

Within the protein environment, the imidazolinone part of the chromophore covalently bonded to a residue and the phenolic-part hydrogen bond to the confined water. Also there these collective motions are significant during the process of phenolic-proton detachment, which happens occurs from the fs to ps time scale.

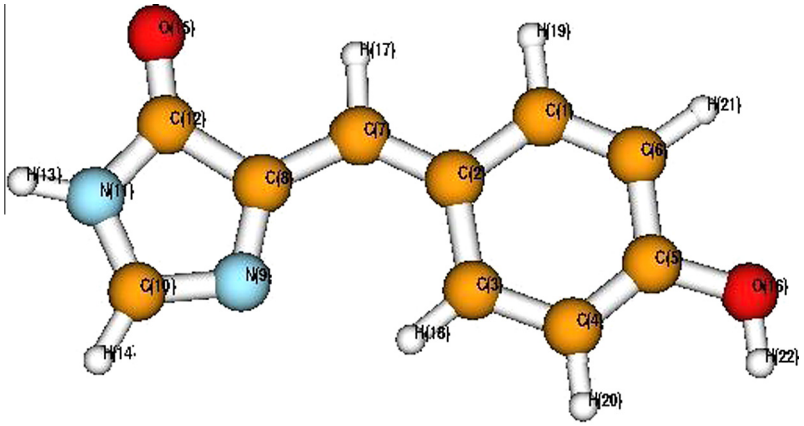

Figure 1. The molecular geometry and atom labelling of the GFP chromophore (*p*-hydroxybenzlidene imidazolinone).

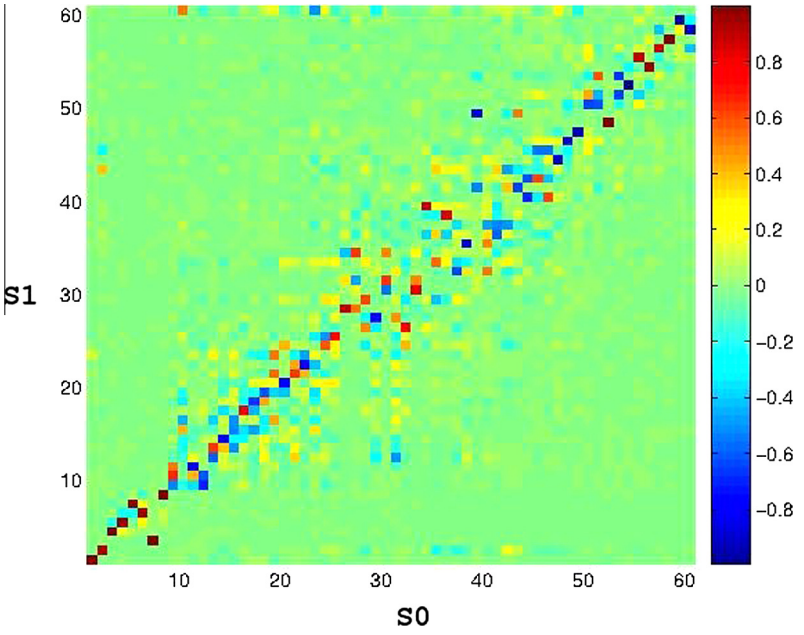

Figure 2. The excited-state (S1) normal modes in terms of the ground state (S0) normal modes.

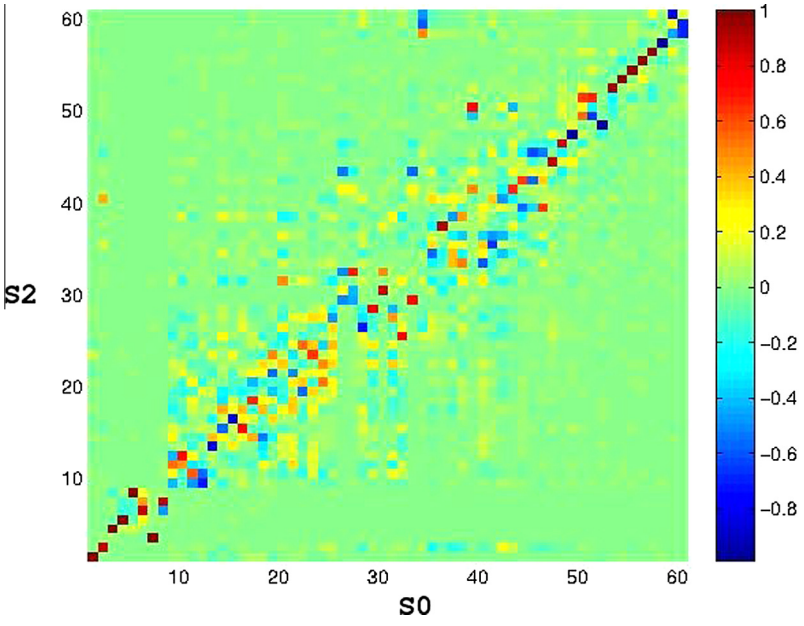

Figure 3. The excited-state (S2) normal modes in terms of the ground state (S0) normal modes.

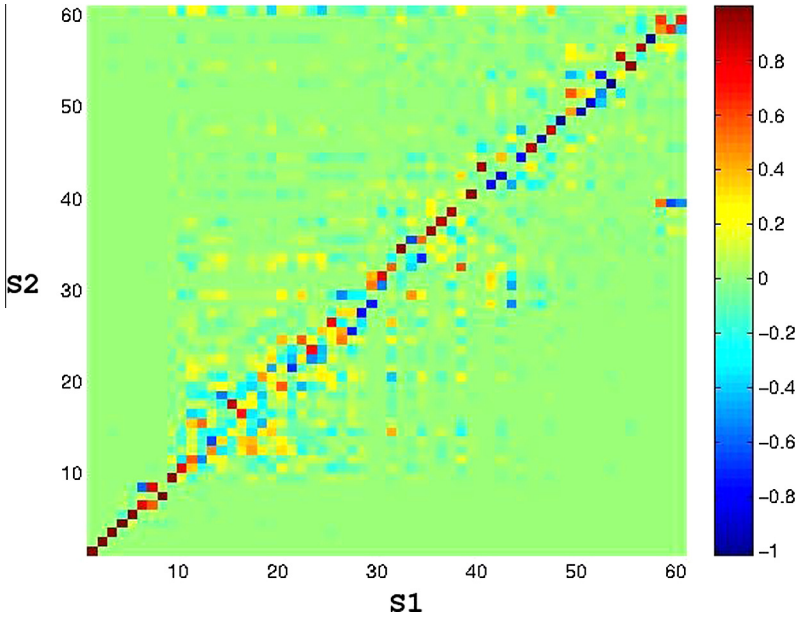

Figure 4. The excited-state (S2) normal modes in terms of the ground state (S1) normal modes.

4. Concluding remarks

We have reported a detailed normal-mode analysis of the GFP chromophore molecule. The experimental frequencies available were matched with the calculated values to provide more information on the modes. We have also made an attempt to understand the mixing of the vibrational modes between different states using the Duschinsky relation. The results have shed light on the detailed contribution of the normal modes to the vibrational cooling from the excited states. We believe the process of mode mixing facilitates the detachment of the proton from the chromophore and to stabilise the system. More quantitative details can be obtained using a higher QM method with the inclusion of anharmonicity [29] to evaluate the vibrational frequencies of the chromophore along with hydrogen bonded water and the neighboring residues such as Ser, Glu, as both of them are coupled during the process of excitation. Depending on the computational power, it would also be valuable to treat the chromphore with the QM method and the rest of the protein with the MM method similar to the method described elsewhere [30,31]. This clarifies the role of the protein matrix during excitation and vibrational relaxation. Hopefully, our analyses provide additional information on previous results [9,10,13–18] and are useful in understanding the process of vibrational relaxation in a qualitative way. It would be nevertheless interesting to consider the vibrational superexchange [32–35] in this process.

Acknowledgements

This letter was part of the Research Project RVO: 61388963 of the Institute of Organic Chemistry and Biochemistry, Academy of Sciences of the Czech Republic. This letter was also supported by the Czech Science Foundation [P208/12/G016]. I thank Professor S. Manogaran for providing the UMAT program for the performance of the normal-mode analysis. I am grateful to Tomas Drsata for his help in the figure preparation in Matlab. My sincere thanks are further owed to the Professor Pavel Hobza for his support.

Appendix A. Supplementary data

Supplementary data associated with this article can be found, in the online version, at http://dx.doi.org/10.1016/j.cplett.2013.09.040.

References

[1] A.A. Pakhomov, V.I. Martynov, Chem. Biol. 15 (2008) 755.
[2] S.J. Remington, Curr. Opin. Struct. Biol. 16 (2006) 714.
[3] R.Y. Tsien, Annu. Rev. Biochem. 67 (1998) 509.
[4] M. Zimmer, Chem. Rev. 102 (2002) 759.
[5] C.W. Cody, D.C. Prasher, W.M. Westler, F.G. Prendergast, W.W. Ward, Biochemistry 32 (1993) 1212.
[6] R. Heim, D.C. Prasher, R.Y. Tsien, Proc. Natl. Acad. Sci. USA 91 (1994) 12501.
[7] M. Chattoraj, B.A. King, G.U. Bublitz, S.G. Boxer, Proc. Natl. Acad. Sci. USA 93 (1996) 8362.
[8] K. Brejc, T.K. Sixma, P.A. Kitts, S.R. Kain, R.Y. Tsien, M. Ormo, S.J. Remington, Proc. Natl. Acad. Sci. USA 94 (1997) 2306.
[9] C. Fang, R.R. Froniera, R. Tran, R.A. Mathies, Nature 462 (2009) 200.
[10] M.D. Donato et al., Phys. Chem. Chem. Phys. 13 (2011) 16295.
[11] K. Winkler, J.R. Lindner, V. Subramaniam, T.M. Jovin, P. Vohringer, Phys. Chem. Chem. Phys. 4 (2002) 1072.
[12] Y. Xu, R. Gnanasekaran, D.M. Leitner, Chem. Phys. Lett. 564 (2013) 78.
[13] X. He, A.F. Bell, P.J. Tonge, JPC B 106 (2002) 6056.
[14] P. Schellenberg, E. Johnson, A.P. Esposito, P.J. Reid, W.W. Parson, JPC B 105 (2001) 5316.
[15] A.P. Esposito, P. Schellenberg, W.W. Parson, P.J. Reid, J. Mol. Struct. 569 (2001) 25.
[16] T. Andruniow, J. Mol. Model. 13 (2007) 775.
[17] M. Almasian, J. Grzetic, G. Berden, B. Bakker, W.J. Buma, J. Oomens, Int. J. Mass Spect. 330–332 (2012) 118.
[18] D.M. Leitner, Chem. Phys. Lett. 530 (2012) 102.
[19] F. Duschinsky, Acta Physicochem. (URSS) 7 (1937) 551.
[20] R.J. Hemley, D.G. Leopold, V. Vaida, M. Karplus, J. Chem. Phys. 82 (1985) 5379.
[21] S. Schumm, M. Gerhards, K. Kleinermanns, J. Phys. Chem. A 104 (2000) 10648.
[22] J.R. Reimers, J. Chem. Phys. 115 (2001) 9103.
[23] R. Borrelli, M. Donato, A. Peluso, Chem. Phys. Lett. 413 (2005) 210.
[24] E. Stendardo, F. Avila Ferrer, F. Santoro, R. Improta, J. Chem. Theory Comput. 8 (2012) 4483.
[25] M.J. Frisch, Gaussian 03, Revision C.02, Gaussian, Inc., Wallingford, CT, 2004.
[26] UMAT, D.F. McIntosh, M.R. Peterson, General Vibrational Analysis System, QCPE 576; Indiana University: Bloomington, IN 47405.
[27] J.P. Merrick, D. Moran, L. Radom, J. Phys. Chem. A 111 (2007) 11683.
[28] G. Ramachandran, S. Manogaran, J. Mol. Struct. Theochem. 766 (2006) 125.
[29] R. Pearman, M. Gruebele, J. Chem. Phys. 108 (1998) 6561.
[30] M. Svensson, S. Humbel, R.D.J. Froese, T. Matsubara, S. Sieber, K. Morokuma, J. Phys. Chem. 100 (1996) 19357.

[31] H.M. Senn, W. Thiel, Angew. Chem. Int. Ed. 48 (2009) 1198.
[32] D.M. Letiner, P.G. Wolynes, Phys. Rev. Lett. 76 (1996) 216.
[33] A.A. Stuchebrukhov, R.A. Marcus, J. Chem. Phys. 98 (1993) 6044.
[34] E.J. Heller, J. Phys. Chem. 99 (1995) 2625.
[35] S. Keshvamurthy, P. Schlagheck, Dynamical Tunneling: Theory and Experiment, Taylor and Francis Press, Boca Raton, 2011.